

FLOW IN THE CROSS-OVER CHANNEL OF A STEAM TURBINE

Petr Kočárník, Slavomír Jirků*

The document deals with the research of flow in the cross-over channel of the high-pressure stage with partial admission of first stage. In the opening part there is a description of the experimental model and the method of measuring flow fields with high velocity gradient using the stereo PIV principle. The second part describes the design of the model inlet part. The third chapter deals with measuring in the cross-over channel outlet slot with no influence of the stator blade cascade of the following stage. The stator blade cascade feedback is described in the fourth part. During all the measurements we observe the influence of the shaft revolution on the flow field at the cross-over channel outlet.

Keywords: cross-over channel, steam turbine, partial admission, blade cascade

Nomenclature

c velocity,	r radial coordinate,	α polar coordinate,
c^* dimensionless velocity,	s curvilinear coordinate,	α_1 blade cascade exit angle,
e degree of admission,	x, y rectangular coordinates,	ε cross section reduction,
q^* dimensionless volume flow density,		φ angle of velocity vector.

1. Introduction

The cross-over channel modifies the flow between the first stage of the turbine with partial admission and the following stage with full admission. The aim of the research described below was to experimentally verify the influence of the partial admission, shaft revolution and the stator blade cascade on the uniformity of the following stage admission. An experimental model of the cross-over channel was made for the case of the symmetrical two-slot admission with the partiality degree $e = 0.3$, which corresponds to the slot opening angle of 54° . The basis for the cross-over channel construction was the high-pressure part drawing of the Škoda steam turbine. The velocity field measurements were performed using the stereo PIV method.

While designing the model we had to respect the dimensions and parameters of the aerodynamic measuring track, workplace technological capabilities and specifications of the PIV measurement method [2], [3]. Construction of the model is obvious from Fig. 1. The model is a modular concept, so it allows us to research more variations of arrangement as well as it enables expected future changes when optimising the arrangement. The model can be divided into two basic parts, i.e. the cross-over channel and the inlet part, which

* Ing. P. Kočárník, Ph.D., doc. Ing. S. Jirků, CSc., Czech Technical University in Prague, Faculty of Electrical Engineering, Department of Electric Drives and Traction, Technická 2, 166 27 Praha 6, Czech Republic

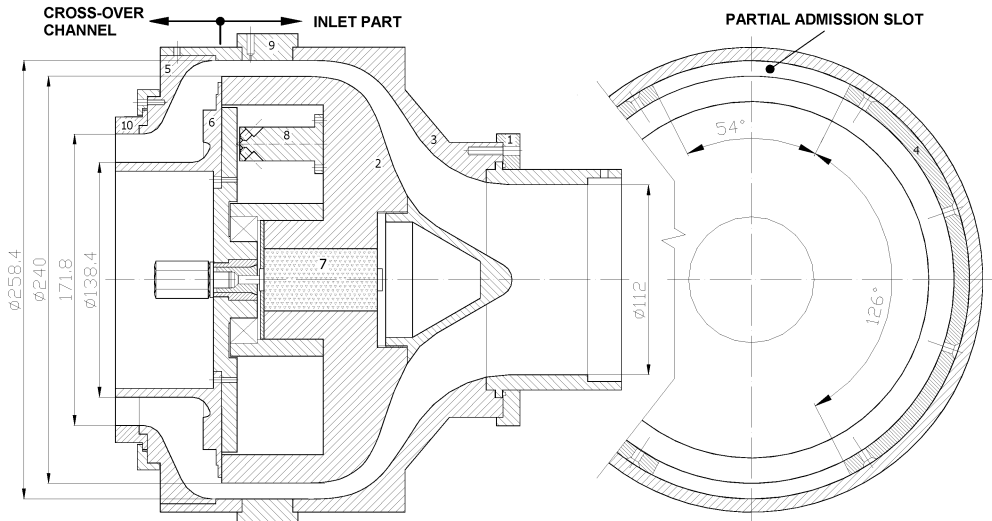


Fig.1: Cross-over channel model

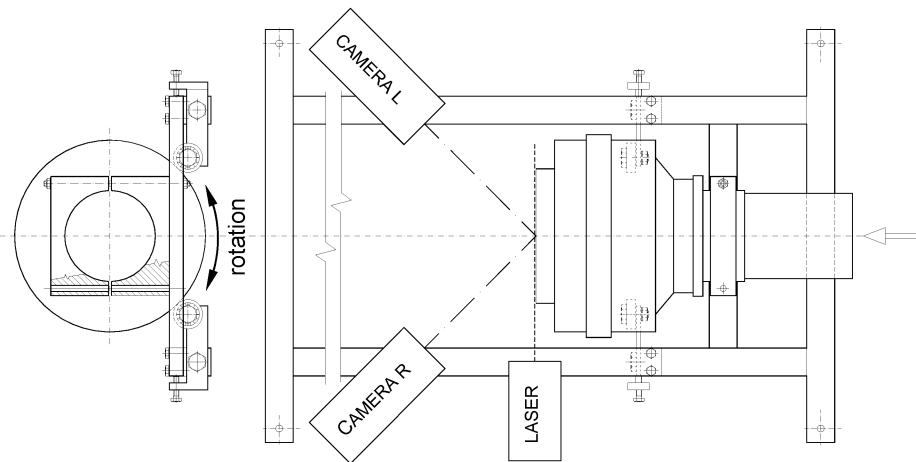


Fig.2: Experiment arrangement

transforms the flow from the measuring track circular pipes to the slots supplying the partial admission. Fig. 2 shows the arrangement of the whole experiment. The inlet part of the model is connected to the aerodynamic track pipeline via rotary flange. Two rotary pulleys support the other side of the part, which allows it to turn round the longitudinal axis. To achieve required resolution the PIV cameras are not able to scan the motion of particles in the whole annular slot, but only in its small part (a sector of about 10° – 24° according to the slot size).

Selected arrangement of the experiment enables successive measuring of velocity fields in the whole slot when the setting of cameras is fixed. The measuring area can be changed by turning the model, but the adjustment of cameras and laser and calibration of the image dimensions must be made before the first measurement only. When the measurement is finished the flow field maps of the whole slot are made up from partial maps using the computing algorithm of the Matlab program.

An electric motor is built in the inlet part area to enable the research on the influence of shaft revolution on the flow field, see Fig. 1. A carrier is attached to the motor shaft with a collet. The inner wall, supplying a part of the shaft in the cross-over channel, is set on the carrier. A revolution measuring incremental sensor is built in the clearance behind the carrier. The electric motor speed regulator is placed outside the model and enables to set revolutions from 0 to 5000 rpm.

On the outer wall there is a shoulder and a flange enabling attachment of different models of blade cascades to allow us to observe the influence of different blade cascades on the cross-over channel flow.

2. Inlet part

The first step of the model construction was to make an inlet part that suitably transforms the flow from the circular pipeline to the annular slot. Regarding its influence on the cross-over channel flow we paid much attention to the design. The form of substantial part of the axially symmetrical duct was designed using the procedure described in [1] so that the maximum dimensions are not exceeded as well as there are no velocity losses in potential flow anywhere on the walls. The left part of Fig. 3 shows selected velocity courses in a planar duct and counted courses accordant with the axially symmetrical duct. The right part shows the final shape of the walls.

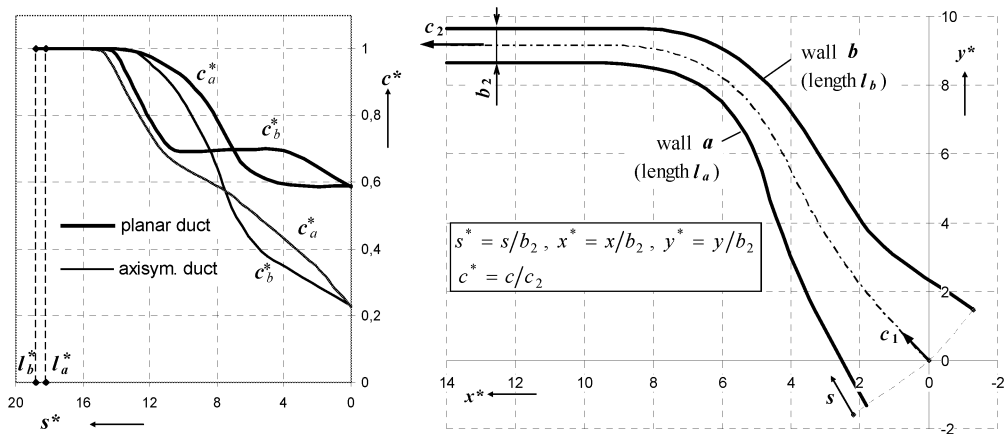


Fig.3: Wall shape design based on the velocity distribution

According to Fig. 1 the designed duct was completed with conical part on the inner wall and circular passage on the outer wall. Its properties were subsequently verified solving the axially symmetrical flow field of viscous fluid in the Fluent program.

The inlet velocity and other parameters were selected so that they correspond to the values supposed in the experiment. With regard to sufficiently flat course of the outlet velocity profile, the axially symmetrical duct designed in this manner was used as a basis for further adjustments.

To supply the partial admission it was necessary to distribute the flow from the whole slot evenly to two sections with specified angle of 54° according to Fig. 1. The easiest adjustment proposal was to insert a simply formed body (hollow cylinder section) with rounded edges

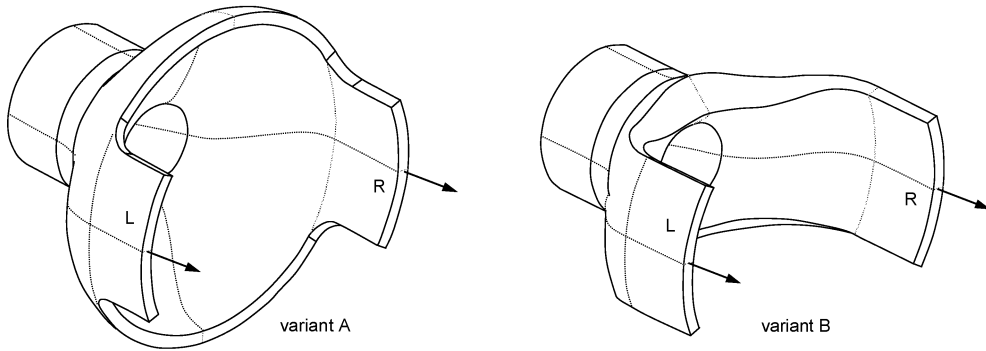


Fig. 4: Flow duct variants

into the straight part of the outlet area. So a duct formed according to Fig. 4, variant A, was created.

A considerable contraction of the cross-section near the outlet indicated unwanted influence on the uniformity of the flow along the outlet slot, which made us change the design to the variant B shown in Fig. 4, where the primarily inserted body was extended with another part almost reaching the inlet pipe so that the flow distribution into slots is displaced further from the outlet.

Numerical models of both variants were solved in Fluent. Fig. 5 shows comparison of velocity profiles along the radial line in symmetrical plane (angle $\alpha = 0^\circ$).

Fig. 6 shows comparison of profiles in a cross section along the middle line of the outlet slot.

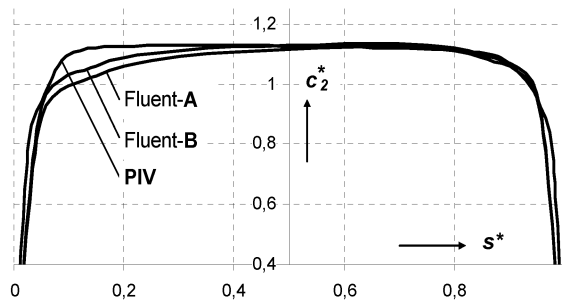


Fig. 5: Velocity profiles along the radial line

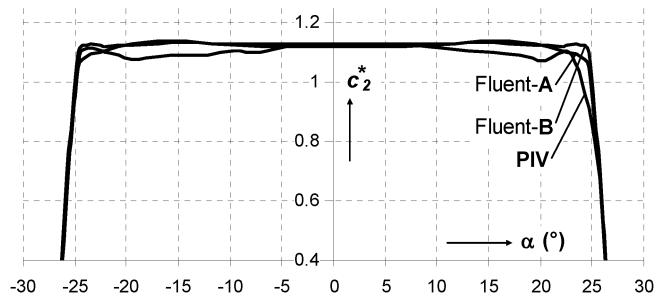


Fig. 6: Velocity profiles along the middle line

With regard to suitable aerodynamic characteristics and especially to considerably easier production of the insert, the A variant was chosen for the model.

The outlet slot flow field was measured via the stereo PIV method. The courses of measured velocity profiles can be also compared with those counted in Figs. 5 and 6.

The distribution of the dimensionless volume flow density in the outlet slot was evaluated as the integral parameter and defined in following relation

$$q^*(\alpha) = \frac{2}{r_E^2 - r_I^2} \int_{r_I}^{r_E} c_2^*(r) r dr . \quad (1)$$

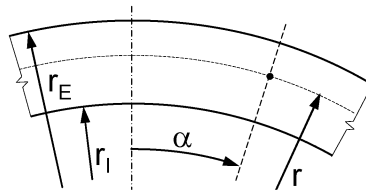


Fig.7: Volume flow density determination

Fig. 7 shows the meaning of individual values; $q^*(\alpha)$ can be also considered as a course of mean value from the radial velocity profiles. Fig. 8 shows the comparison of $q^*(\alpha)$ for individual cases.

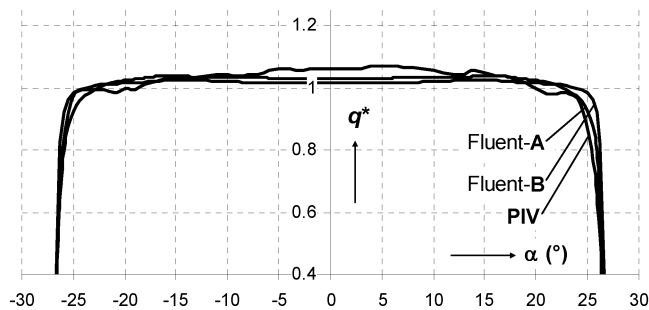


Fig.8: Layout of the dimensionless volume flow density

Variant B provides the best result and can be considered as a reference variant for specified geometric layouts. The $q^*(\alpha)$ distribution mean-square deviation from the Fluent solution for this variant is 3.3 %, while with variant A it is 6.7 %. From the PIV measurement on the inlet part model the $q^*(\alpha)$ distribution deviations in both outlet slots were 8.2 % and 7.5 %.

3. Cross-over channel

Fig. 1 shows the cross-over channel form. The duct inner wall corresponds to the stepwise-shouldered turbine shaft; the outer wall profile consists of circular and straight passages. The first experiments were made with free outlet slot (i.e. without the stator blade cascade) and, in addition, the influence of the inner wall rotation (turbine shaft) on the outlet slot velocity field was monitored. This influence was researched using four selected modes set by

the ratio of the inner wall circumferential velocity at the inlet slot (approx. the first-stage blade circumferential velocity) and the inlet slot flow velocity. In the experiments performed the ratio λ was 0; 0.5; 1 and 1.5. When the mean inlet velocity was 31 m/s, there were 0, 1225, 2550 and 3825 rpm on the inner wall.

According to the measurements performed the aggregate fields of dimensionless components of velocity along the outlet slot were set and presented in Figs. 9, 10 and 11. The mean value of axial velocity in the outlet was taken as the velocity standard.

Fig. 9 shows the comparison of the fields of axial velocity components. The isotaches layout shows that most of the flow is concentrated at the area corresponding to the position of partial admission. An undesired separation of the flow behind the final bend at the area of maximum flow as well as the backflow is also obvious. In all cases of nonzero rotation of the inner wall the influence of the wall on the flow field layout is evident. A small deformation in the direction of rotor revolution is present at just $\lambda = 0.5$, see, for example, the area given by the isotach -0.1 . For the anticipated operation mode at $\lambda = 1$ the influence of revolution is not so significant. The deformation of the axial velocity component field is important when the ratio λ increase to 1.5.

Fig. 10 shows the comparison of the fields of tangential velocity components. The isotaches layout evidently confirms the undesired state, where the tangential velocity component changes its sign. In cases of the inner wall rotation the isotaches layout shows the fact that the higher the λ value is, the smaller are those areas, where the fluid flows against the shaft rotation (i.e. reduction of areas with positive value of the tangential component).

Fig. 11 shows the comparison of the fields of radial velocity components. Compared to other components, size of this component is much smaller. However, the higher the λ value

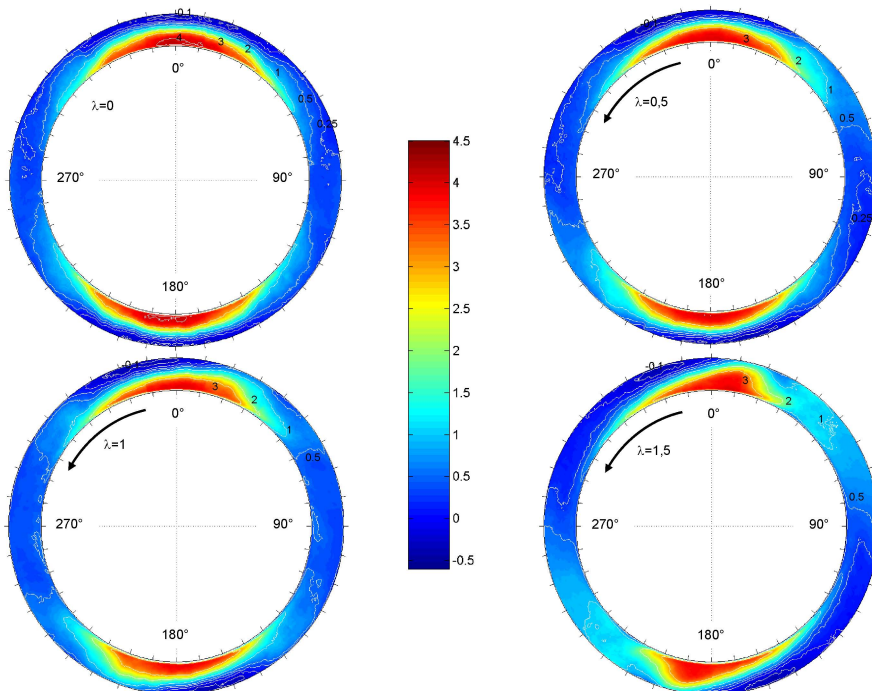


Fig.9: Fields of axial velocity components

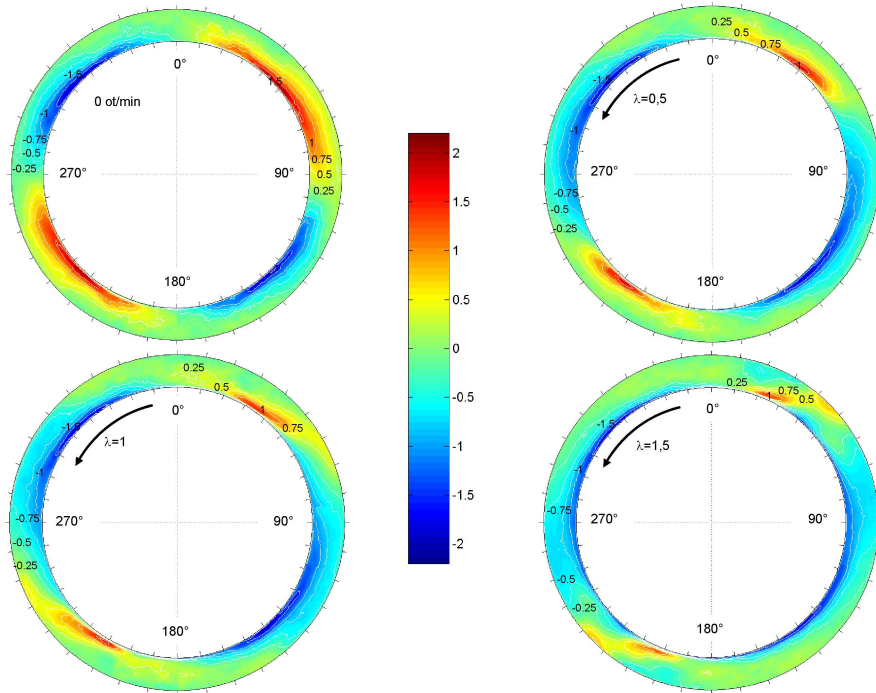


Fig.10: Fields of tangential velocity components

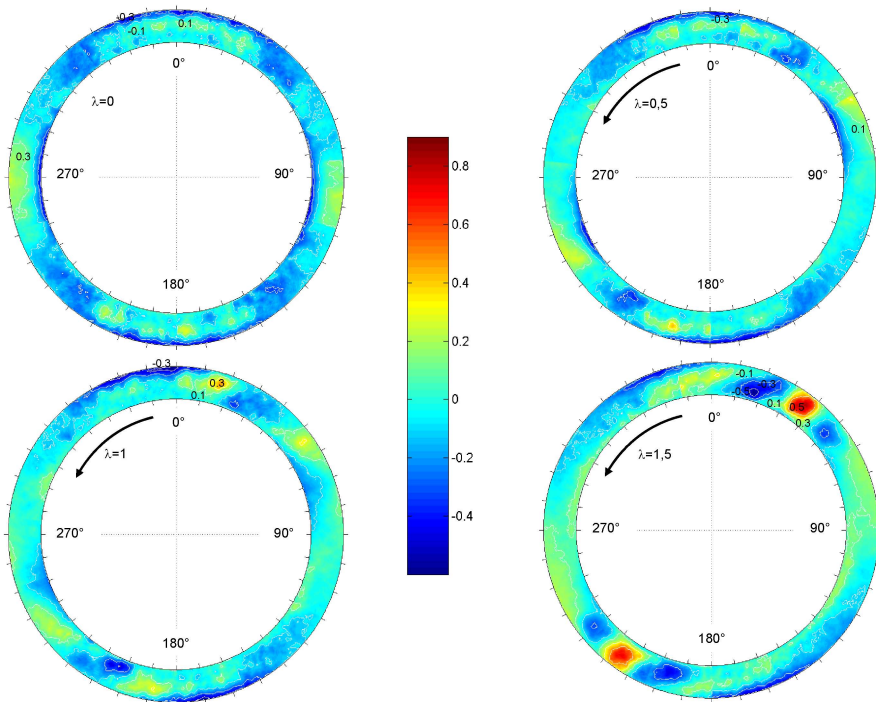


Fig.11: Fields of radial velocity components

is, the more deformed is the velocity field. At $\lambda = 1.5$ it leads to formation of two remarkable ‘focal points’ in the flow field, where the fluid is expelled from the slot in radial direction more intensively.

The courses of layouts of the dimensionless volume flow density $q^*(\alpha)$ along the outlet slot are shown in Fig. 12 for all four cases of the λ ratio. The course of $q^*(\alpha)$ at zero revolutions confirms significant and undesired variation within the range of 0.3–2.0. The other $q^*(\alpha)$ courses with the inner wall revolution show that the negative influence of revolution becomes more evident not until $\lambda = 1.5$.

According to specified $q^*(\alpha)$ courses a mean-square deviation was counted for further comparison. For the values under this research $\lambda = 0; 0.5; 1$ and 1.5 the deviation is 57.3%; 60.6%; 60.4% and 74.1%.

Fig. 13 shows the layout of mean values of the outlet velocity vector angle along the outlet slot. The φ angle is defined by the ratio of mean values of the tangential and axial velocity components. At zero revolutions of the inner wall the $\varphi(\alpha)$ angle vary from about -65° to 65° . The other courses representing the revolution influence show that there is positive decrease of areas with positive φ angle value.

Mean values for the φ angle in the whole slot for the λ values of $\lambda = 0; 0.5; 1; 1.5$ are $1.5^\circ, -21.9^\circ, -20^\circ$ and -28.7° , which confirms the positive influence of revolution.

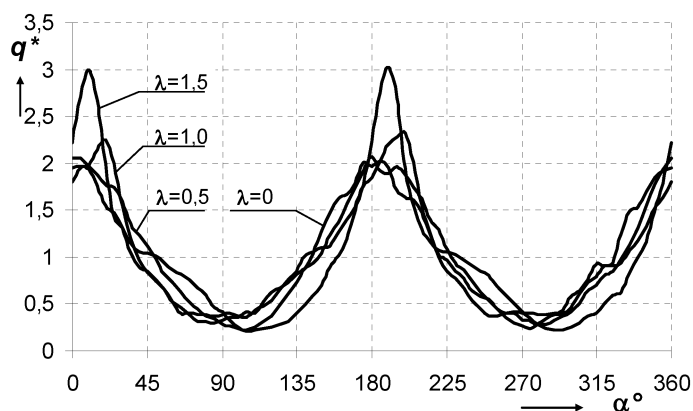


Fig.12: Layout of the volume flow density

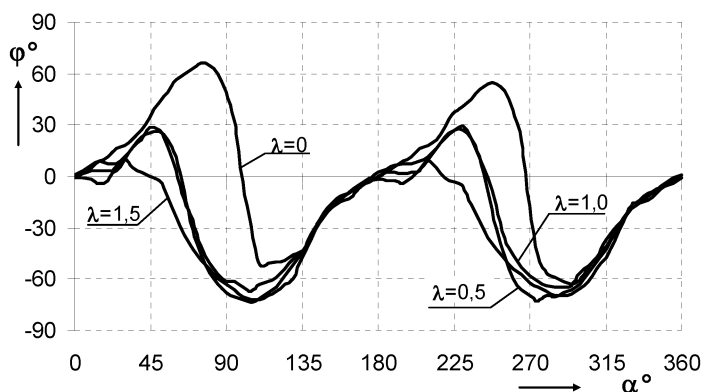


Fig.13: Course of the $\varphi(\alpha)$ angle mean values

4. Blade cascade

The cross-over channel flow is significantly influenced by the existing following stage, which creates continuous resistance for flowing liquid. This resistance causes improvement of uniformity of the cross-over channel outlet flow. Its size is obviously affected by the resistance of the stator blade cascade and can be defined by means ε of reduction of cross-sections of the individual impeller passages. This reduction is defined by the ratio of blade cascade throat width to the blade spacing $o/t = \sin \alpha_1$ and the ratio of trailing edge length to the leading edge length l_o/l_n , (see Fig. 14)

$$\varepsilon = \frac{l_o}{l_n} \sin \alpha_1 . \tag{2}$$

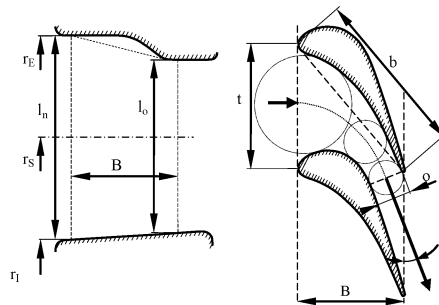


Fig.14: Geometric characteristics of the stator blade cascade

The backward influence of the blade cascade on the cross-over channel flow was researched in two cases of substitute blade cascade, whose geometric dimensions are shown in Figs. 15 and 16.

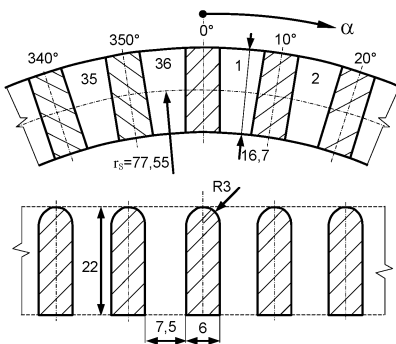


Fig.15: Substitute blade cascade A

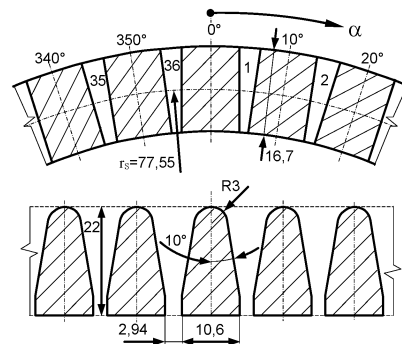


Fig.16: Substitute blade cascade B

There are 36 blades in both variants. The reduction of the flow duct cross-section for variant A is $\varepsilon = 0.55$, for variant B it is $\varepsilon = 0.22$. If the ratio is $l_o/l_n = 0.8$, the reduction of the flow duct cross-section corresponds to the outlet angle of $\alpha_1 = 33^\circ$ in variant A and $\alpha_1 = 16^\circ$ in variant B for the real blade cascade.

The velocity field in the outlet slot was measured in both variants of the substitute blade cascade. The experiments were made at the same mean velocity in the inlet and for the

same ratios λ of velocities like in previous measurement. The mean value of axial velocity in the outlet impeller slots was used as the velocity standard for the layout of velocity fields.

Fig. 17 shows of the axial outlet velocity component for $\lambda = 0$ in both variants of the blade cascade. It is evident that in variant A with reduction $\varepsilon = 0.55$ the blade cascade influence on the flow uniformity is low. In the second case with reduction $\varepsilon = 0.22$ the flow is significantly more even. From the velocity fields layout we can see that in both blade cascade cases the flow is not separated behind the last cross-over channel bend.

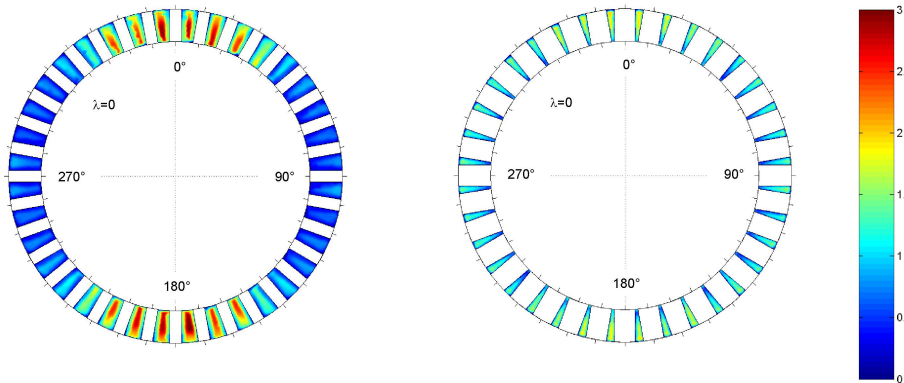


Fig.17: Fields of the axial velocity components

Figs. 18 and 19 shows the layout of mean density of the volume flow in the impeller passages $q^*(\alpha)$ for all λ values. From the courses in both charts it is evident that the influence of the inner wall revolution on the $q^*(\alpha)$ volume flow density layout is not probative for any of the substitute blade cascade cases.

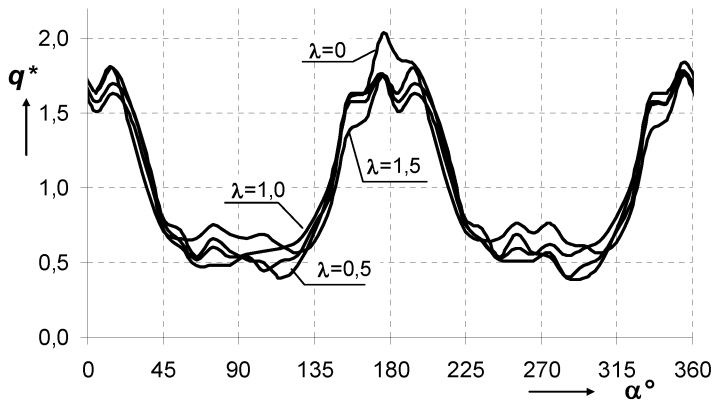


Fig.18: $q^*(\alpha)$ density comparison for blade cascade A

Fig. 20 shows the comparison of layouts of the dimensionless volume flow densities $q^*(\alpha)$ for $\lambda = 0$ between the free outlet case and both variants of the substitute blade cascade. All courses are shown as functions of the dimensionless slot length. The courses confirm significant evenness of the flow in the blade cascade variant B with reduction of the flow duct cross-section $\varepsilon = 0.22$.

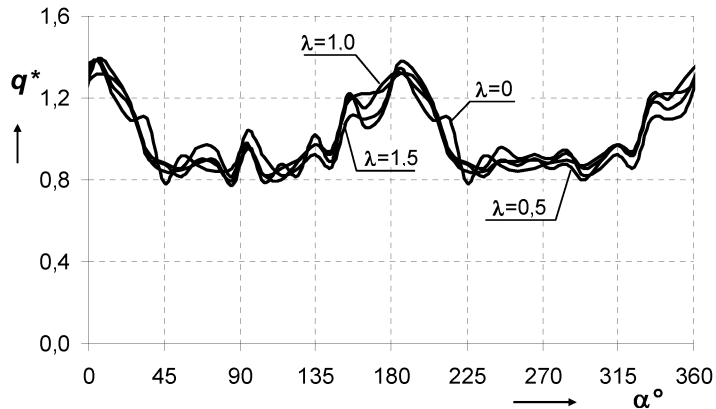


Fig.19: $q^*(\alpha)$ density comparison for blade cascade B

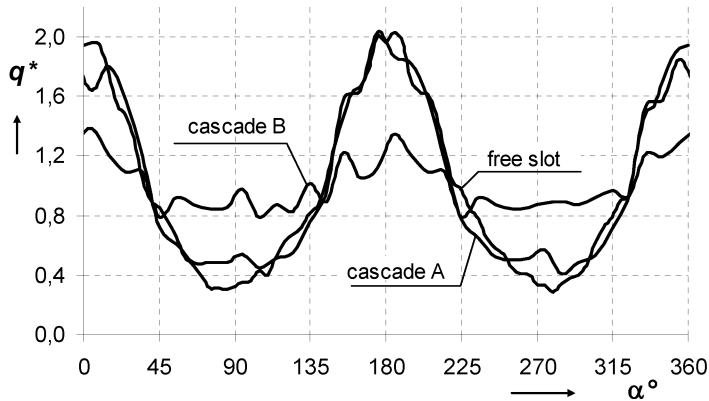


Fig.20: $q^*(\alpha)$ comparison

5. Conclusion

The flow in the cross-over channel behind the partial admission stage has essential influence on the evenness of the following stage admission (as well as other stages, if needed). The measurements performed show that reduction of the flow duct cross-section in the stator blade cascade of this stage has the essential influence on the uniformity of this stage flow. However, the uniformity of leading angle, which changes within the range of $\pm 65^\circ$ along the circumference, is still a substantial problem.

The research on the influence of the inner wall revolution on the cross-over channel flow shows that the revolution influences the outlet velocity field layout only if there is no stator blade cascade built-in the outlet. This is probably caused by the fact that after its separation behind the last bend the flow shortly cleaves to the rotating wall. There is no separation in case no blade cascade is used, the flow layout is more even and, in addition, stator blades narrowly surround this part of rotating wall so that this effect cannot apply.

Presented research met a lot of objectives. First of all, a variable cross-over channel model was developed. Then, the stereo PIV methodology was established for measuring in narrow slots with high velocity gradient and the measurement processing algorithms were debugged. While designing the inlet part, the usability of fast optimising method for thin

flow duct shape was verified as well as its use along with the Fluent program. Series of measurements associated with the flow identification were performed on this experimental model. Their results are the basis for determination of the numeric model parameters.

Currently, we are working on optimisation of the cross-over channel shape so as to eliminate the above-mentioned unevenness of the leading flow angle.

References

- [1] Kočárník P., Jirků S.: The Design of Annular Bend in Spiral Casing of the Low-pressure Part Steam Turbines. In Proceedings of 6th European Conference on Turbomachinery – Fluid Dynamics and Thermodynamics. Lille: Ecole Nationale Supérieure d' Arts et Métiers, 2005, vol. 1, 2, pp. 510–520
- [2] Novotný J., Čížek J., Matěcha J., Adamec J.: Accuracy of Stereo – PIV Measurement, In: 21st Danubia-Adria Symposium on Experimental Methods in Solid Mechanics, Zagreb: Croatian Society of Mechanics, 2004, pp. 44–45
- [3] Raffel M., Willert C.E., Kompenhans J.: Particle Image Velocimetry. Springer Verlag, Berlin Heidelberg, 1998
- [4] Willinger R., Pikbougoum M.: Effect of Partial Admission on the Flow Field in the Wheel Chamber of an Industrial Steam Turbine, In: Proceedings of 6th European Conference on Turbomachinery – Fluid Dynamics and Thermodynamics, Lille: Ecole Nationale Supérieure d' Arts et Métiers, 2005, vol. 1, 2, pp. 436–448.
- [5] Bohn D., Gier J., Ziemann M.: Einfluß der überströmgehäusegeometrie auf den Strömungsausgleich bei Turbinen mit Teilbeaufschlagung, VGB KraftwerksTechnik 2/98, pp. 62–68, Deutschland, Februar 1998
- [6] Horlock J.H.: Axial Flow Turbines: Fluid Mechanics and Thermodynamics, Krieger Pub Co, 1973
- [7] Traupel W.: Thermische Turbomaschinen: Erster Band. Thermodynamisch-strömungstechnische Berechnung, Springer, 2000.
- [8] Traupel W.: Thermische Turbomaschinen: Zweiter Band, Geänderte Betriebsbedingungen, Regelung, Mechanische Probleme, Temperaturprobleme, Springer, 2000

Received in editor's office: April 23, 2009

Approved for publishing: March 23, 2010